

On the radial density profile of intracluster gas tracing the isothermal dark halo with a finite core

Xiang-Ping Wu and Yan-Jie Xue

Beijing Astronomical Observatory and National Astronomical Observatories, Chinese Academy of
Sciences, Beijing 100012; China

Received April 6 2000; accepted June 3 2000

ABSTRACT

The cusped NFW universal density profile suggested by typical CDM models has been challenged in recent years by the discoveries of the soft cores with finite central density for a broad range of masses from dwarf galaxies to clusters of galaxies. It is thus desirable that a new, analytic model would instead become available for virialized dark halos. One promising candidate is probably the empirical density profile proposed by Burkert (1995), which resembles an isothermal profile with a constant core in the inner region and matches the NFW profile at large radii. Meanwhile, such a revised dark halo (RDH) profile has turned out a great success on galactic scales. This stimulates us to apply the RDH profile to more massive systems like clusters of galaxies. In this paper we have made an attempt to derive the radial density profile of intracluster gas from the RDH profile under the isothermal and hydrostatic equilibrium hypotheses, and compare it with those revealed by X-ray observations and inferred from the NFW profile. It is shown that the RDH predicted gas density can be well represented by the conventional β model with a typical β parameter of $\beta \sim 0.7\text{--}0.9$. Alternatively, fitting the theoretically predicted X-ray surface brightness profile to an ensemble of 45 X-ray clusters observed by ROSAT, we find that the RDH and NFW profiles become to be almost indistinguishable from each other, and their characteristic density and scale length parameters are strongly correlated. Yet, unlike the NFW model, the RDH profile can allow us to work out straightforwardly the central dark matter density from X-ray measurements of the surface brightness and temperature of clusters. It appears that the resulted central densities of the 45 clusters have an average value of $\langle \rho_0 \rangle \approx 0.01 \text{ M}_\odot \text{ pc}^{-3}$, in agreement with the result estimated on galactic scales, which reinforces the claim for the presence of the soft halo cores over the entire mass range.

Subject headings: cosmology: theory — dark matter — galaxies: clusters: general — X-rays: galaxies

1. Introduction

For decades many efforts have been made towards the understanding of the radial density profile of intracluster gas from the well-motivated physical mechanism, in an attempt to recover the empirical β model (Cavaliere & Fusco-Femiano 1976) which fits nicely the X-ray observed surface brightness distribution of clusters. Assuming both galaxies and gas are the tracers of the shape and depth of a common gravitational potential of a cluster, Cavaliere & Fusco-Femiano (1976, 1978) obtained an analytic gas density profile resembling the β model in shape if the King model is used to represent the galaxy number density profile in the inner cluster region. In recent years, the rapid progress of numerical simulating techniques has permitted the reconstruction of the dark matter halos with an unprecedented resolution, ranging from galactic scales of ~ 1 kpc to large-scale structures of ~ 10 Mpc. This leads one to view the issue at a different angle: Given the gravitational potential wells defined by the dark halos, how is the intracluster gas distributed in clusters if the hydrostatic equilibrium between the gas and the underlying gravitational potentials has been built up? In particular, much attention has been paid to the issue of how to reconstruct the radial gas density and temperature profiles if the dark halos follow the so-called universal density profile (Navarro, Frenk & White 1995; NFW) suggested by high-resolution simulations within the framework of typical CDM models such as SCDM, LCDM and Λ CDM (Makino, Sasaki & Suto 1998; Suto, Sasaki & Makino 1998; Yoshikawa & Suto 1999; Wu & Chiueh 2000). It turns out that there is indeed a striking similarity between the predicted X-ray surface brightness profiles of clusters and the conventional β model. This has stimulated several authors to apply the NFW predicted X-ray surface brightness profiles to the observed ones for an ensemble of X-ray clusters (Makino & Asano 1999; Ettori & Fabian 1999; Wu & Xue 2000; Wu 2000).

Yet, besides its uncomfortable singularity at $r = 0$, the cusped NFW profile has been shown to be in conflict with observations (e.g. Tyson, Kochanski & Dell’Antonio 1998; Navarro & Steinmetz 2000; Firmani et al. 2000; and references therein). In fact, it has been noticed that, while the NFW profile yields a gas density profile close to the empirical β model, the core radius predicted by the cusped density profile may be smaller than the actually observed one (Makino

et al. 1998). Moreover, the NFW profile leads to an increasing gas temperature towards cluster centers (Wu & Chiueh 2000), in contrast with the presence of the cold gas components detected very often inside the X-ray cores. Motivated by the soft inner matter distributions of the dark halos revealed observationally from dwarf galaxies to rich clusters, Spergel & Steinhardt (2000) recently proposed that the CDM particles are self-interacting. As a result, the collisional CDM particles, in a similar way to the baryonic particles, will produce the less centrally concentrated structures. This weakly self-interacting CDM model has soon attracted many investigations, among which the numerical simulations of structure formation based on some simple physical consideration of the self-interacting CDM particles have successfully provided a scenario that is essentially consistent with the existing observations (Hannestad 1999; Burkert 2000 and references therein).

As a natural extension, one may address the following question: Does there exist a similar analytic expression to the NFW universal density profile that one can use to approximately describe the matter distribution of the virialized dark halos resulted from the weakly self-interacting CDM model ? A conclusive answer to such a question seems not easy: Unlike the standard CDM particles, for which there is no need to consider the interaction between particles except their gravity, the collisional, warm CDM particles contain an unknown parameter, the cross-section. Consequently, even with the help of high-resolution simulations, it is still hard to completely determine the final configurations of dark halos. Under present circumstances, one promising candidate is probably the empirical density profile suggested by Burkert (1995):

$$\rho_{DM}(r) = \frac{\rho_0 r_0^3}{(r + r_0)(r^2 + r_0^2)}, \quad (1)$$

where ρ_0 and r_0 are the central density and the scale length, respectively. This revised dark halo (RDH) density law resembles an isothermal profile in the inner region with a constant core r_0 , while in the outer region the mass profile diverges logarithmically with r , in agreement with the NFW profile. So, such a density profile does have the desired properties at the central and outermost regions. In particular, it fits fairly well the dark matter distributions of dwarf galaxies revealed by both the rotation curves and the numerical simulations of evolution of halos consisting

of weakly self-interacting CDM particles (Burkert 2000; Salucci & Burkert 2000).

Motivated by the apparent success of the RDH profile of eq.(1) on galactic scales and the possible existence of weak interaction between CDM particles, in this paper we would like to apply the RDH profile to more massive systems like clusters of galaxies. We would like to demonstrate the radial density profile of intracluster gas tracing the gravitational potential defined by the RDH profile, and compare the expected X-ray surface brightness with the X-ray observations and other models (e.g. the conventional β model and that predicted by the NFW profile), although we have an intuition that the RDH profile, as a combination of the NFW profile and the β model, would provide an essentially similar result. This study will nevertheless constitute an important test for the universality of the RDH profile as the virialized dark halos over the entire mass range, and will also allow us to examine whether there are any common properties in the NFW and RDH profiles. Eventually, it is hoped that this study will be useful for a conclusive answer to the question as to whether the RDH profile can be used to replace the role of the NFW profile for the virialized dark halos, if CDM particles are indeed weakly self-interacting.

2. Density profile of intracluster gas

2.1. Self-gravity of the gas: excluded

If the dark halo of a cluster follows the RDH profile described by eq.(1), the total dark matter enclosed within radius r is

$$M_{DM}(x) = 4\pi\rho_0 r_0^3 \tilde{m}(x); \quad (2)$$

$$\tilde{m}(x) = \frac{1}{2} \left[\ln(1+x) + \frac{1}{2} \ln(1+x^2) - \arctan(x) \right], \quad (3)$$

where $x = r/r_0$. Assuming that the intracluster gas is isothermal (with a temperature of T) and in hydrostatic equilibrium with the underlying gravitational potential dominated by M_{DM} , we have

$$\frac{GM_{DM}(x)}{x^2} = -\frac{kTr_0}{\mu m_p n_{gas}(x)} \frac{dn_{gas}(x)}{dx}, \quad (4)$$

in which $n_{gas}(x)$ is the gas number density and μ is the average molecular weight. Note that we have neglected the self-gravity of the gas for the moment. A straightforward computation yields an analytic form of gas density profile:

$$\frac{n_{gas}(x)}{n_{gas}(0)} = \left[e^{-(1+\frac{1}{x}) \arctan x} (1+x)^{(1+\frac{1}{x})} (1+x^2)^{\frac{1}{2}(\frac{1}{x}-1)} \right]^{\frac{\alpha_0}{2}}, \quad (5)$$

where

$$\alpha_0 = \frac{4\pi G \mu m_p \rho_0 r_0^2}{kT}. \quad (6)$$

In order to avoid the divergence of the resulting X-ray surface brightness to be discussed below because of $n_{gas}(\infty) = n_{gas}(0)e^{-\pi\alpha_0/4}$, in a similar way to the treatment of the NFW predicted gas density profile (see Wu 2000), we introduce a normalized, background subtracted gas number density $\tilde{n}_{gas}(x) \equiv [n_{gas}(x) - n_{gas}(\infty)]/[n_{gas}(0) - n_{gas}(\infty)]$, which reads

$$\tilde{n}_{gas}(x) = \frac{1}{e^{\frac{\pi\alpha_0}{4}} - 1} \left\{ \left[e^{\frac{\pi}{2} - (1+\frac{1}{x}) \arctan x} (1+x)^{(1+\frac{1}{x})} (1+x^2)^{\frac{1}{2}(\frac{1}{x}-1)} \right]^{\frac{\alpha_0}{2}} - 1 \right\}. \quad (7)$$

Another way to deal with the non-zero background gas density predicted by the dark halo model is to truncate the cluster at a certain radius (e.g. the virial radius) as adopted by Makino et al. (1998). It is indeed unfortunate that one has to add an arbitrary, unphysical constraint on the gas density profile to ensure the convergence of the X-ray surface brightness.

In Fig.1 we demonstrate the radial profiles of the scaled gas density $\tilde{n}_{gas}(x)$ for typical clusters with $\alpha_0 = 5, 10$ and 20 . A glimpse of Fig.1 seems to suggest that all the resulted profiles of $\tilde{n}_{gas}(x)$ resemble the conventional β models in shape. We then overlap the β model, $\tilde{n}_{gas}^*(x) = [1 + (x/x_c)^2]^{-3\beta/2}$, to each curve with $(\beta, r_c/r_0) = (0.40, 0.86), (0.74, 0.85)$ and $(1.56, 0.92)$ for $\alpha_0 = 5, 10$ and 20 , respectively, where $x_c = r_c/r_0$ is the scaled core radius. Yet, like the actual fitting of the β model to the X-ray observed surface brightness profile, the best-fit β parameters depend also on the extension of the fitting regions. For a typical cluster of $\alpha_0 \approx 10$, the best-fit β value over a region out to $10r_c$ is $\beta \approx 0.7$, in good agreement with X-ray observations. In particular, the gas core radius takes roughly the value of r_0 . Also plotted in Fig.1 are the

corresponding gas densities predicted by the NFW profile with $\alpha = \alpha_0$ (Makino et al. 1998; Wu 2000)

$$\tilde{n}_{gas}(x) = \frac{(1+x)^{\alpha/x} - 1}{e^\alpha - 1}, \quad (8)$$

where $x = r/r_s$ and $\alpha = 4\pi G\mu m_p \rho_s r_s^2 / kT$. A visual examination of Fig.1 reveals that there are some differences between the expected radial variation of intracluster gas from the RDH profile and that from the NFW profile, which are reflected not only by the significantly different scale lengths but also by the different shape. Indeed, it is unlikely that the two types of density profiles can be made to be identical simply by a horizontal replacement. Whether these differences are significantly important will be discussed when the two density profiles are both applicable to an ensemble of X-ray clusters (section 3).

EDITOR: PLACE FIGURE 1 HERE.

2.2. Self-gravity of the gas: included

The total mass in gas within radius x is simply

$$M_{gas}(x) = 4\pi\mu m_p r_0^3 \int_0^x n_{gas}(x) x^2 dx. \quad (9)$$

When the self-gravity of the gas is included, the hydrostatic equation becomes

$$\frac{G[M_{DM}(x) + M_{gas}(x)]}{x^2} = -\frac{kTr_0}{\mu m_p n_{gas}(x)} \frac{dn_{gas}(x)}{dx}. \quad (10)$$

If we introduce the volume-averaged (gas) baryon fraction $f_b(x)$ as a new variable:

$$f_b(x) = \frac{M_{gas}(x)}{M_{DM}(x) + M_{gas}(x)}, \quad (11)$$

we can obtain the following two first-order differential equations

$$\frac{d\bar{n}_{gas}}{dx} = -\alpha_0 \frac{\tilde{m}\bar{n}_{gas}}{(1-f_b)x^2}; \quad (12)$$

$$\frac{df_b}{dx} = \frac{(1-f_b)[b(1-f_b)\bar{n}_{gas} - f_b\tilde{\rho}_{DM}]x^2}{\tilde{m}}, \quad (13)$$

where $\bar{n}_{gas} = n_{gas}(x)/n_{gas}(0)$, $b = \mu m_p n_{gas}(0)/\rho_0$ and $\tilde{\rho}_{DM} = \rho_{DM}/\rho_0 = (1+x)^{-1}(1+x^2)^{-1}$. We need to specify the boundary conditions in order to solve the above equations. The first condition is obviously

$$\bar{n}_{gas}(0) = 1. \quad (14)$$

Following the recent work of Wu & Chiueh (2000), we choose the boundary condition of $f_b(x)$ such that the baryon fraction within the virial radius r_{vir} (or $c = r_{vir}/r_0$) should asymptotically approach the universal value $f_{b,BBN} = \Omega_b/\Omega_M$, where Ω_b and Ω_M are, respectively, the baryon and total mass densities of the Universe in units of the critical density ρ_c for closure, namely,

$$f_b(c) = f_{b,BBN}; \quad (15)$$

$$\left. \frac{df_b}{dx} \right|_{x=c} = 0. \quad (16)$$

Here the scaled virial radius or the so-called concentration parameter c is defined by

$$M_{DM}(c) = \frac{4\pi}{3} r_0^3 \rho_c c^3 \Delta_c, \quad (17)$$

or

$$\frac{\tilde{m}(c)}{c^3} = \frac{\Delta_c}{3} \frac{1}{\delta_c}, \quad (18)$$

in which $\delta_c = \rho_0/\rho_c$, and Δ_c represents the overdensity parameter of dark matter with respect to the average background value ρ_c and will be taken to be 200 in our computation below.

The free parameters involved in eqs.(12) and (13) and the boundary conditions are α_0 , b , $f_{b,BBN}$ and c or δ_c . However, there are only two independent parameters with the restrictions of eqs.(15) and (16), which we choose to be δ_c and $f_{b,BBN}$ below. We will perform the numerical searches for the solutions of eqs.(12) and (13) under the boundary conditions of eqs.(14)–(16). Technically, we search for the solutions over a two-parameter space (α_0, b) by iterations until the boundary conditions are satisfied, which enables us to work out the radial profiles of gas density and baryon fraction, together with a unique determination of the parameters α_0 and b . In Fig.2 we demonstrate a set of solutions for two typical choices of $f_{b,BBN}$ and δ_c : $f_{b,BBN} = (0.05, 0.1)$ and $\delta_c = (10^4, 10^5)$, and the resulting α_0 and b values are listed in Table 1. It appears that the derived

density profiles of the baryon fraction exhibit no dramatic variation over the whole clusters: For a small value of $\delta_c \sim 10^4$, f_b increases slightly with outward radius and eventually matches the background value at virial radius, while for a large $\delta_c \sim 10^5$, f_b would reach a maximum before approaching asymptotically the universal value. The parameter α_0 also acts roughly like a constant (~ 12) even if the characteristic density δ_c changes by a decade, and the parameter b turns out to be an increasing function of $f_{b,BBN}$, which arises simply from $b \propto \mu m_p n_{gas}(0)$. Now, we concentrate on the derived profiles of gas density. All the predicted density curves of intracluster gas shown in Fig.2 seem to well resemble the β models, which is illustrated by our superimposed β model onto each of the derived density profiles. The most remarkable feature is that the corresponding values of β and core radius have all fallen into very narrow ranges of $0.87 < \beta < 0.98$ and $0.65 < r_c/r_0 < 0.88$ for our choices of the universal baryon fraction $f_{b,BBN}$ and the characteristic density δ_c for typical clusters (see Table 1). An increase of δ_c up to 10^6 , the roughly largest density for clusters (see next section), only leads to a minor modification to these limits. This indicates that the isothermal gas in different clusters should essentially follow a similar distribution, i.e., the observationally determined β among different clusters should not show a large scatter around the mean value $\beta \sim 0.9$. Note that the gas core radius r_c may vary substantially because of the different r_0 for different clusters. While the predicted density profile of intracluster gas demonstrates a property basically consistent with what has been known for X-ray clusters, the theoretically expected β parameter is likely to slightly exceed the presently determined one from X-ray observation, $\beta \approx 0.7$. The former arises mainly from our restriction that the baryon fraction should asymptotically match the background value. Previous studies with this constraint have also arrived at a similar conclusion: the β value in the β model for intracluster gas is required to be larger than a certain low-limit (Wu & Chiueh 2000). Actually, it is not impossible that the presently fitted β parameters based on the X-ray observed surface brightness profiles of clusters are biased low because of the influence of the cooling-flows and the small fitting regions. Excluding the cooling flows or adopting a double β model fit may moderately raise the observationally determined β values, giving rise to $\beta \approx 0.7\text{--}0.8$ (Vikhlinin et al. 1999; Xue & Wu 2000). Of course, the present computation has been made within the framework of isothermality,

and the above prediction cannot be taken too literally unless the non-isothermal gas is included.

EDITOR: PLACE FIGURE 2 HERE.

Considering the fact that f_b exhibits only a minor variation over the whole cluster, and also for illustrating the effect of the self-gravity of the gas, we can provide an approximate and analytic form of the gas density by taking $f_b = f_{b,BBN}$ in eqs.(12) and (13). Consequently, eq.(12) reduces to eq.(4) and the gas density is given by the analytic expression eq.(7), in which the parameter α_0 is now replaced by $\alpha_0^* = \alpha_0/(1 - f_b)$. In Table 1, we list the β parameters and core radii in the β model fits to our approximate solutions using the same input values of $f_{b,BBN}$ and δ_c (or α_0). In the case of the low density $\delta_c = 10^4$, the agreement between the exact and approximate solutions is fairly good, while the approximate solutions seem to underestimate the β values by ~ 0.15 for $\delta_c = 10^5$. The latter is partially due to the fact that the fitting of the β model is made over rather a large region out to $x = c = 14.2$, where a shallower density profile occurs according to the RDH profile (see Fig.1). Another reason is that in the case of $\delta_c = 10^4$, the baryon fraction remains roughly unchanged across the clusters with a relative variation rate of $|f_b(c) - f_b(0)|/f_{b,BBN} < 20\%$, in comparison with $|f_b(c) - f_b(0)|/f_{b,BBN} \sim 100\%$ for $\delta_c = 10^5$. Namely, the small δ_c clusters seem to meet more easily the condition for the approximate solutions ($f_b = f_{b,BBN}$) than the large δ_c clusters do. Nevertheless, we conclude that the derived gas distributions with and without the inclusion of the self-gravity of the gas do not show very significant difference, and in general, the self-gravity of the gas only leads to a slightly steeper gas density profile as a result of the increase of the underlying gravitational mass. This is consistent with the similar study for the NFW profile (Suto et al. 1998).

3. Application to X-ray clusters

In this section we conduct a comparison between our derived gas density profile and X-ray observations, which are linked up through the X-ray surface brightness profiles of clusters, S_x . In

the scenario of the optically thin, isothermal plasma emission,

$$S_x(x) \propto \int_x^\infty \tilde{n}_{gas}^2 d\ell, \quad (19)$$

where the integral is performed along the line of sight ℓ . Here we take the analytic form of the gas density eq.(7) and neglect the contribution of the gas self-gravity. We intend to fit our theoretically expected X-ray surface brightness profile eq.(19) to an ensemble of the X-ray observed surface brightness profiles of clusters, which will allow us to determine the characteristic parameters, ρ_0 and r_0 , for the RDH profile and compare them with the results from other models, e.g. the β model and the NFW profile.

We use the ROSAT PSPC observed surface brightness profiles of 45 nearby clusters compiled by Mohr, Mathiesen & Evrard (1999, MME). Several models have been already tested with this sample, such as the β model, the double β model and the NFW predicted density profile (MME; Wu & Xue 2000; Xue & Wu 2000). In a similar way to our previous analysis for the NFW profile (Wu & Xue 2000), we perform the χ^2 -fit to get the best-fit parameters α_0 and r_0 , in which we keep the same outer radii of the fitting regions as those defined by MME. In order to examine how our results are affected by the presence of the cooling flows in some clusters, we perform our fittings by using the entire data points of S_x (model A) and excising the central region of 0.05 Mpc in each cluster (model B), respectively. For the latter the reason that we adopt the same inner radius for all the clusters is to guarantee the uniformity of the excision (Markevitch 1998). We then compute ρ_0 in terms of eq.(6) by taking the X-ray temperature data from the literature (see Wu, Xue & Fang 1999; and references therein). For majority of the clusters we use the cooling flow corrected temperature data by White (2000). In Fig.3 we illustrate a typical example of the observed and our fitted surface brightness profiles (model A) for cluster A3158. For comparison, we have also plotted the results of the β model and the NFW profile. Essentially, these three models provide more or less an equal goodness of fit to the observed data with $\chi_\nu^2 = 1.12, 1.24$ and 1.10 for the β model, the NFW and RDH profiles, respectively. From the fitting of the X-ray surface brightness profile alone, it may be hard to reject any of these models. In Table 2 we list the best-fit values of ρ_0 and r_0 for the 45 MME clusters by model A, together with the results for the β model and

the NFW profile, in which all the quoted errors are 68% confidence limits. The Hubble constant is taken to be $H_0 = 50 \text{ km s}^{-1} \text{ Mpc}^{-1}$. When the central regions of 0.05 Mpc are excised in the fittings, the best-fit parameters for all the three models are only moderately affected. However, this can significantly improve the goodness of the fittings characterized by the reduced χ^2_ν : After the excision of the central regions (model B), the fractions of clusters with $\chi^2_\nu \leq 2$ increase from (10/45, 14/45, 7/45) to (26/45, 25/45, 22/45) for (β , NFW, RDH) models, respectively. Recall that the similar fraction of 26/45 is found by MME for the single β and double β model fittings. It appears that about half of the clusters cannot be well fitted by any of these models even if the central regions are excised.

EDITOR: PLACE FIGURE 3 HERE.

3.1. RDH vs. β model

We first analyze the possible link between the RDH profile and the β model. For this purpose we plot in Fig.4 the best-fit α_0 vs. β and r_0 vs. r_c for the 45 MME clusters obtained by model A. It is immediate that there exist strong correlations between the scale and slope parameters in the two models. We fit these correlations to a power-law function, which reads

$$\alpha_0 = 10^{1.08 \pm 0.01} \beta^{0.67 \pm 0.06}, \quad (\text{A}); \quad (20)$$

$$\alpha_0 = 10^{1.10 \pm 0.01} \beta^{0.86 \pm 0.04}, \quad (\text{B}), \quad (21)$$

and

$$r_0 = 10^{-0.071 \pm 0.015} r_c^{0.75 \pm 0.02}, \quad (\text{A}); \quad (22)$$

$$r_0 = 10^{-0.033 \pm 0.012} r_c^{0.83 \pm 0.01}, \quad (\text{B}). \quad (23)$$

Meanwhile, applying a linear fit to the data set yields

$$\alpha_0 = (14.11 \pm 1.09)\beta, \quad (\text{A}); \quad (24)$$

$$\alpha_0 = (13.44 \pm 0.55)\beta, \quad (\text{B}), \quad (25)$$

and

$$r_0 = (1.46 \pm 0.41)r_c, \quad (\text{A}); \quad (26)$$

$$r_0 = (1.30 \pm 0.18)r_c, \quad (\text{B}). \quad (27)$$

It appears that the resultant relationships with and without the excision of the central regions in the fits of the X-ray observed surface brightness profiles are roughly consistent with each other.

EDITOR: PLACE FIGURE 4 HERE.

3.2. NFW vs. β model

For comparison we display in Fig.5 the correlations between the corresponding parameters in the NFW profile and the β model. The best-fit α - β and r_s - r_c relations using all the 45 data points are

$$\alpha = 10^{1.28 \pm 0.02} \beta^{1.46 \pm 0.08}, \quad (\text{A}); \quad (28)$$

$$\alpha = 10^{1.36 \pm 0.02} \beta^{1.81 \pm 0.08}, \quad (\text{B}), \quad (29)$$

and

$$r_s = 10^{0.64 \pm 0.03} r_c^{1.03 \pm 0.03}, \quad (\text{A}); \quad (30)$$

$$r_s = 10^{0.77 \pm 0.02} r_c^{1.27 \pm 0.02}, \quad (\text{B}). \quad (31)$$

However, there are four clusters, A119, A1367, A1656 and A2255 showing a large dispersion on the α - β plane, which may significantly affect the above fittings. The best-fit α - β relation without these four clusters becomes

$$\alpha = 10^{1.16 \pm 0.01} \beta^{1.01 \pm 0.03}, \quad (\text{A}); \quad (32)$$

$$\alpha = 10^{1.41 \pm 0.06} \beta^{1.26 \pm 0.01}, \quad (\text{B}). \quad (33)$$

Alternatively, the linear fit to the data set of 45 clusters gives

$$\alpha = (15.40 \pm 2.83)\beta, \quad (\text{A}); \quad (34)$$

$$\alpha = (15.23 \pm 2.54)\beta, \quad (\text{B}), \quad (35)$$

and

$$r_s = (4.17 \pm 1.19)r_c, \quad (\text{A}); \quad (36)$$

$$r_s = (3.70 \pm 1.06)r_c, \quad (\text{B}). \quad (37)$$

Within the uncertainties, the last four relations are consistent with the findings by Ettori & Fabian (1999) based on 36 high-luminosity clusters: $\alpha = 14.34\beta$ and $r_s = 3.17r_c$.

EDITOR: PLACE FIGURE 5 HERE.

3.3. RDH vs. NFW

We now compare the RDH and NFW profiles. Fig.6 shows the correlations between the density and length scale parameters in the two models. Applying the χ^2 -fit with the inclusion of the measurement uncertainties to the data set gives

$$\left(\frac{\rho_0}{\rho_c}\right) = 10^{1.97 \pm 0.06} \left(\frac{\rho_s}{\rho_c}\right)^{0.73 \pm 0.02}, \quad (\text{A}); \quad (38)$$

$$\left(\frac{\rho_0}{\rho_c}\right) = 10^{2.18 \pm 0.06} \left(\frac{\rho_s}{\rho_c}\right)^{0.66 \pm 0.01}, \quad (\text{B}), \quad (39)$$

and

$$r_0 = 10^{-0.54 \pm 0.01} r_s^{0.71 \pm 0.02}, \quad (\text{A}); \quad (40)$$

$$r_0 = 10^{-0.54 \pm 0.01} r_s^{0.64 \pm 0.02}, \quad (\text{B}). \quad (41)$$

The average ratios of ρ_0/ρ_s and r_0/r_s are, respectively,

$$\rho_0 = (8.63 \pm 5.61)\rho_s, \quad (\text{A}); \quad (42)$$

$$\rho_0 = (7.89 \pm 4.93)\rho_s, \quad (\text{B}), \quad (43)$$

and

$$r_0 = (0.36 \pm 0.09)r_s, \quad (\text{A}); \quad (44)$$

$$r_0 = (0.37 \pm 0.10)r_s, \quad (\text{B}). \quad (45)$$

The last two relations are consistent with the estimate of Burkert (2000), $r_0 \approx 0.2r_s$, for dwarf galaxies. The existence of these strongly positive correlations is helpful for us to make a quantitative comparison between the two models. Indeed, from their predicted gas densities, and in turn their X-ray surface brightness profiles of clusters, along with the correlations between the characteristic density and scale length parameters, we are unable to distinguish the two models as the dark halos of clusters. However, there is a remarkable difference, the central density. In fact, the characteristic density parameters, ρ_0 and ρ_s , in these two models have very different meanings. ρ_0 represents explicitly the central density of dark matter, while the parameter ρ_s corresponds to the density nowhere in clusters. Note that the large error bars in the linear ρ_0 - ρ_s relation (eqs.[42] and [43]) and the average values of ρ_s and ρ_0 listed in Table 2 are mainly due to the inclusion of a very few clusters (e.g. A262 and A3526) whose X-ray surface brightness profiles show two distinct length scales

EDITOR: PLACE FIGURE 6 HERE.

3.4. Central dark matter density

Recall that the disagreement between the shallower central density profiles required by various observations with the cusped density profile provided by the NFW model is one of the primary motivations for advocating the scenario of the weakly interacting dark matter particles (Spergel & Steinhardt 2000). A combination of the RDH profile and the X-ray surface brightness measurements of clusters can now allow us to determine straightforwardly the central dark matter densities (ρ_0) of clusters. It is easy to show that ρ_0 is related to the central total mass density $\rho_{\beta,0}$

inferred from the conventional isothermal β model through

$$\rho_{\beta,0} = \frac{9\beta kT}{4\pi G\mu m_p r_c^2} = 9 \left(\frac{\beta}{\alpha_0} \right) \left(\frac{r_0}{r_c} \right)^2 \rho_0. \quad (46)$$

Using the linear relations established above between α_0 , β , r_0 and r_c , we have $\rho_{\beta,0} \approx \rho_0$. Of course, the good agreement between $\rho_{\beta,0}$ and ρ_0 could be interpreted as the consequence of the common working hypothesis behind the two models: The intracluster gas is assumed to be isothermal and in hydrostatic equilibrium with the underlying gravitational potential. In a recent work, Firmani et al. (2000) have demonstrated an essentially constant central density of dark halos for a broad range of masses from dwarf galaxies to clusters of galaxies. However, there are only three data points on cluster scales which are derived from gravitational lensing. Now, we superimpose our derived central densities of dark halos of the 45 MME clusters on their illustration of halo central density vs. maximum rotation velocity (Fig.7), in which the velocity dispersion is plotted as the horizontal axis for clusters. Although the central densities of the clusters span almost two decades from 10^{-3} to $10^{-1} \text{ M}_{\odot} \text{ pc}^{-3}$, the average value $\langle \rho_0 \rangle = 0.012 \text{ M}_{\odot} \text{ pc}^{-3}$ ($0.006 \text{ M}_{\odot} \text{ pc}^{-3}$ for model B) is in agreement with the one ($0.02 \text{ M}_{\odot} \text{ pc}^{-3}$) reported by Firmani et al. (2000). This reinforces the claim for the presence of the soft halo cores over the entire mass range.

EDITOR: PLACE FIGURE 7 HERE.

4. Discussion and conclusions

None of the present numerical simulations based on typical CDM models can reproduce the soft cores of dark halos detected observationally in various systems from dwarf and low surface brightness galaxies to clusters of galaxies. This challenges the analytic and elegant form of the universal density profile suggested by NFW as the virialized dark halos. Without a sophisticated treatment of the dynamical evolution of the CDM particles, we have made an attempt to adopt the empirical density profile (RDH) proposed by Burkert (1995) to replace the cusped NFW profile for dark halos. The RDH profile with a finite core r_0 has been shown to give a perfect fit

to the observed rotation curves of dwarf galaxies. In particular, it also provides an excellent fit to the dark matter distributions revealed by numerical simulations (Burkert 2000) in the scenario that the CDM particles are weakly self-interacting, suggested recently to overcome the difficulties of CDM models (Spergel & Steinhardt 2000). In the present paper we have applied the RDH profile to clusters of galaxies and derived the radial distribution of intracluster gas under the isothermal and hydrostatic equilibrium hypotheses. It turns out that the RDH resulted gas density resembles the conventional β model, although a slightly large β parameter ($\beta \sim 0.7\text{--}0.9$) may be required. The latter nevertheless agrees with the results usually found by numerical simulations (e.g. NFW; Eke, Navarro & Frenk 1998), and is also marginally consistent with the β model fit by excising the cooling flow regions (e.g. Vikhlinin et al. 1999) or adopting an additional β model for the central X-ray emission (Xue & Wu 2000). Except for the very differently asymptotic behaviors at $r \rightarrow 0$, the RDH and NFW profiles become to be almost indistinguishable from each other within the extent of the current X-ray observations of clusters. By fitting the RDH predicted X-ray surface brightness profile to the observed one for an ensemble of 45 clusters, we have estimated the typical central density ρ_0 and core radius r_0 in the RDH profile, which show a fairly strong correlation with the characteristic density ρ_s and scale parameter r_s in the NFW profile, respectively. Meanwhile, our derived central dark matter densities of the 45 clusters have an average value of $\langle \rho_0 \rangle \approx 0.01 \text{ M}_\odot \text{ pc}^{-3}$, in agreement with the result estimated on galactic scales (Firmani et al. 2000).

Yes, a conclusive justification for whether the RDH profile can be used as a good approximation of dark halos and therefore, replace the role of the NFW profile for typical CDM models will be provided by high-resolution simulations incorporated with new physical mechanism for dark matter particles such as the weak self-interaction. Several new models with the help of numerical simulations are being constructed by a number of authors. It can be predicted that a new analytic model with an isothermal core, if it is not the RDH profile, for the structure of virialized dark halos will soon be available. The rotation curves of dwarf galaxies, the total mass distribution of clusters revealed by gravitational lensing, and the X-ray properties of clusters as explored in the present paper will constitute a critical test for the new RDH profile.

This work was supported by the National Science Foundation of China, under Grant 19725311.

Table 1. Numerical results for typical clusters

$f_{b,BBN}$	δ_c	c	α_0	b	β	r_c/r_0	β^*	$(r_c/r_0)^*$
0.05	10^4	5.48	12.0	0.05	0.867	0.705	0.90	0.66
0.05	10^5	14.2	13.7	0.09	0.974	0.681	0.83	0.68
0.10	10^4	5.48	10.8	0.09	0.927	0.884	0.90	0.63
0.10	10^5	14.2	12.8	0.23	0.981	0.649	0.83	0.68

*The β model fit to the approximate solution eq.(7) by assuming $f_b = f_{b,BBN}$ and replacing α_0 by $\alpha_0/(1 - f_{b,BBN})$.

REFERENCES

- Burkert, A., 1995, ApJ, 447, L25
- Burkert, A., 2000, ApJ, submitted (astro-ph/0002409)
- Cavaliere, A., & Fusco-Femiano, R., 1976, A&A, 49, 137
- Cavaliere, A., & Fusco-Femiano, R., 1978, A&A, 70, 677
- Eke, V. R., Navarro, J. F., & Frenk, C. S., 1998, ApJ, 503, 569
- Ettori, S., & Fabian, A. C., 1999, MNRAS, 305, 834
- Firmani, C., D’Onghia, E., Avila-Reese, V., Chincarini, G., & Hernández, X., 2000, MNRAS, in press
- Hannestad, S., 1999, preprint astro-ph/9912558
- Makino, N., & Asano, K., 1999, ApJ, 512, 9
- Makino, N., Sasaki, S., & Suto, Y., 1998, ApJ, 497, 555
- Markevitch, M., 1998, ApJ, 503, 77
- Mohr, J. J., Mathiesen, B., & Evrard, A. E., 1999, ApJ, 517, 627 (MME)
- Navarro, J. F., Frenk, C. S., & White, S. D. M., 1995, MNRAS, 275, 720 (NFW)
- Navarro, J., F., & Steinmetz, M., 2000, ApJ, 528, 607
- Salucci, P., & Burkert, A., 2000, ApJ, in press
- Spergel, D. N., & Steinhardt, P. J., 2000, Phys. Rev. Lett., in press
- Suto, Y., Sasaki, S., & Makino, N., 1998, ApJ, 509, 544
- Tyson, J. A., Kochanski, G. P., & Dell’Antonio, I. P., 1998, ApJ, 498, L107
- Vikhlinin, A., Forman, W., & Jones, C., 1999, ApJ, 525, 47
- White, D. A., 2000, MNRAS, 312, 663
- Wu, X.-P., 2000, MNRAS, in press

- Wu, X.-P., & Chiueh, T., 2000, ApJ, submitted
- Wu, X.-P., & Xue, Y.-J., 2000, ApJ, 529, L5
- Wu, X.-P., Xue, Y.-J., & Fang, L.-Z. 1999, ApJ, 524, 22
- Xue, Y.-J., & Wu, X.-P., 2000, MNRAS, submitted
- Yoshikawa, K., & Suto Y., 1999, ApJ, 513, 549

Fig. 1.— The radial density profiles of intracluster gas derived from the RDH profiles (solid lines) and the superimposed β models (open squares). The parameters (α_0 , β , r_c/r_0) are: (a)-(5, 0.40, 0.86), (b)-(10, 0.74, 0.85) and (c)-(20, 1.56, 0.92). For comparison, the NFW predicted results (dotted lines) are also shown with $\alpha = \alpha_0$. The horizontal scales are r/r_0 and r/r_s for the RDH and NFW profiles, respectively.

Fig. 2.— Numerical solutions of gas density and baryon fraction, when the self-gravity of the gas is included, for two choices of the central density $\delta_c = \rho_0/\rho_c$ and the universal baryon fraction $f_{b,BBN}$. The best-fit β model to each curve is plotted as open squares. The corresponding parameters are summarized in Table 1.

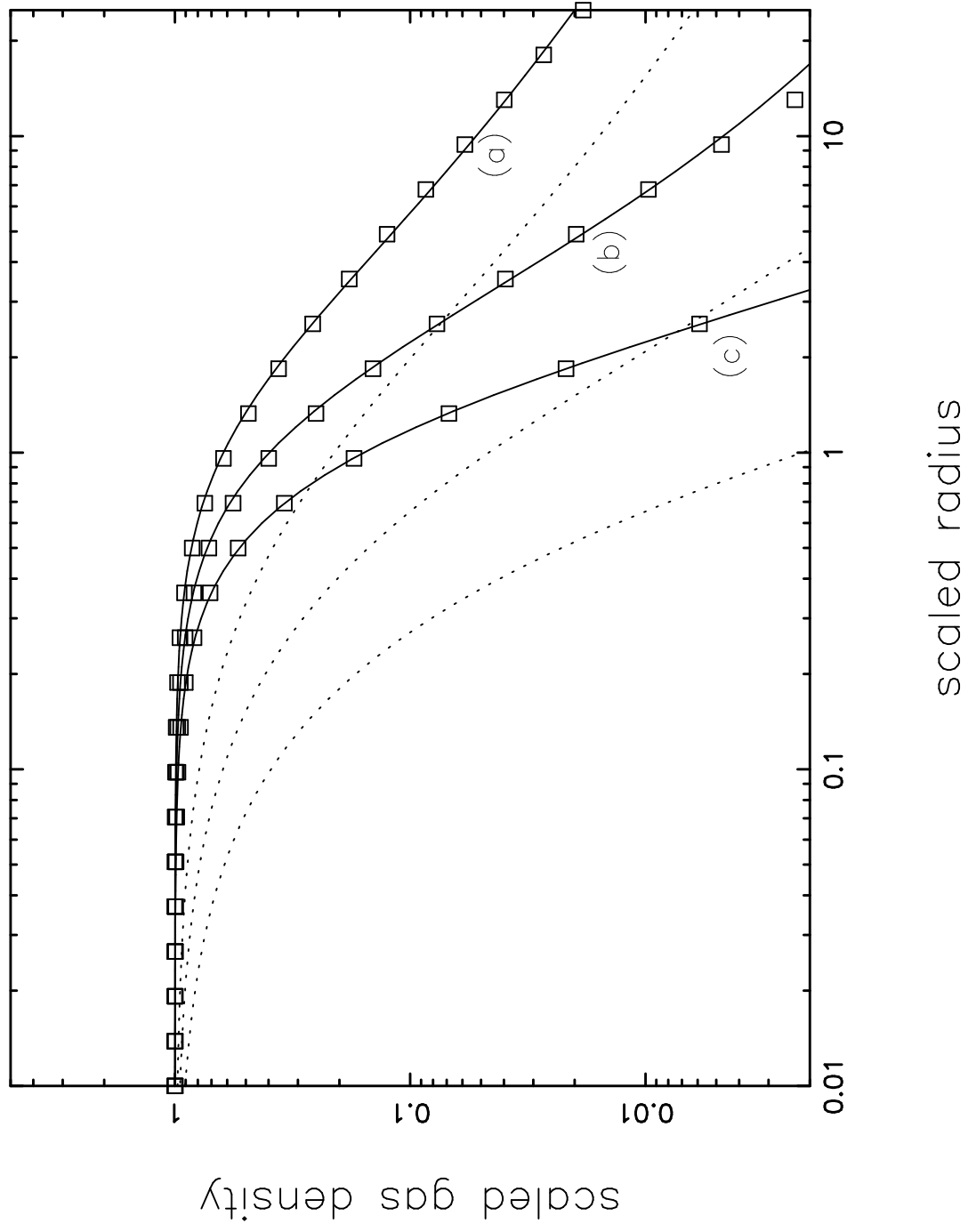
Fig. 3.— An example of the observed and predicted X-ray surface brightness profiles S_x for A3158. Filled circles: the ROSAT PSPC observed data; Open squares: the best-fit β model; Dashed line: the NFW predicted result; Solid line: the RDH result. Residuals between the best-fit of the RDH profile and the data are illustrated in upper panel.

Fig. 4.— Correlations between the slope and scale parameters in the RDH profile and β model determined from the 45 MME clusters. The solid lines are the best-fit relations.

Fig. 5.— The same as Fig.4 but for NFW profile and β model. The dotted line shows the best-fit relation by excluding A119, A1367, A1656 and A2255.

Fig. 6.— Correlations between the density and scale parameters in the RDH and NFW profiles derived from the 45 MME clusters. The solid lines represent the best-fit relations.

Fig. 7.— Central density of dark halos on scales from galaxies to clusters of galaxies. We take the data for dwarf galaxies (filled squares), LSB galaxies (open squares) and three distant clusters (open circles) from the work of Firmani et al. (2000) directly. Our derived central densities ρ_0 in the RDH profile for 45 MME clusters are shown by filled circles, for which the horizontal axis represents velocity dispersion rather than maximum rotation velocity (V_m) as for galaxies.



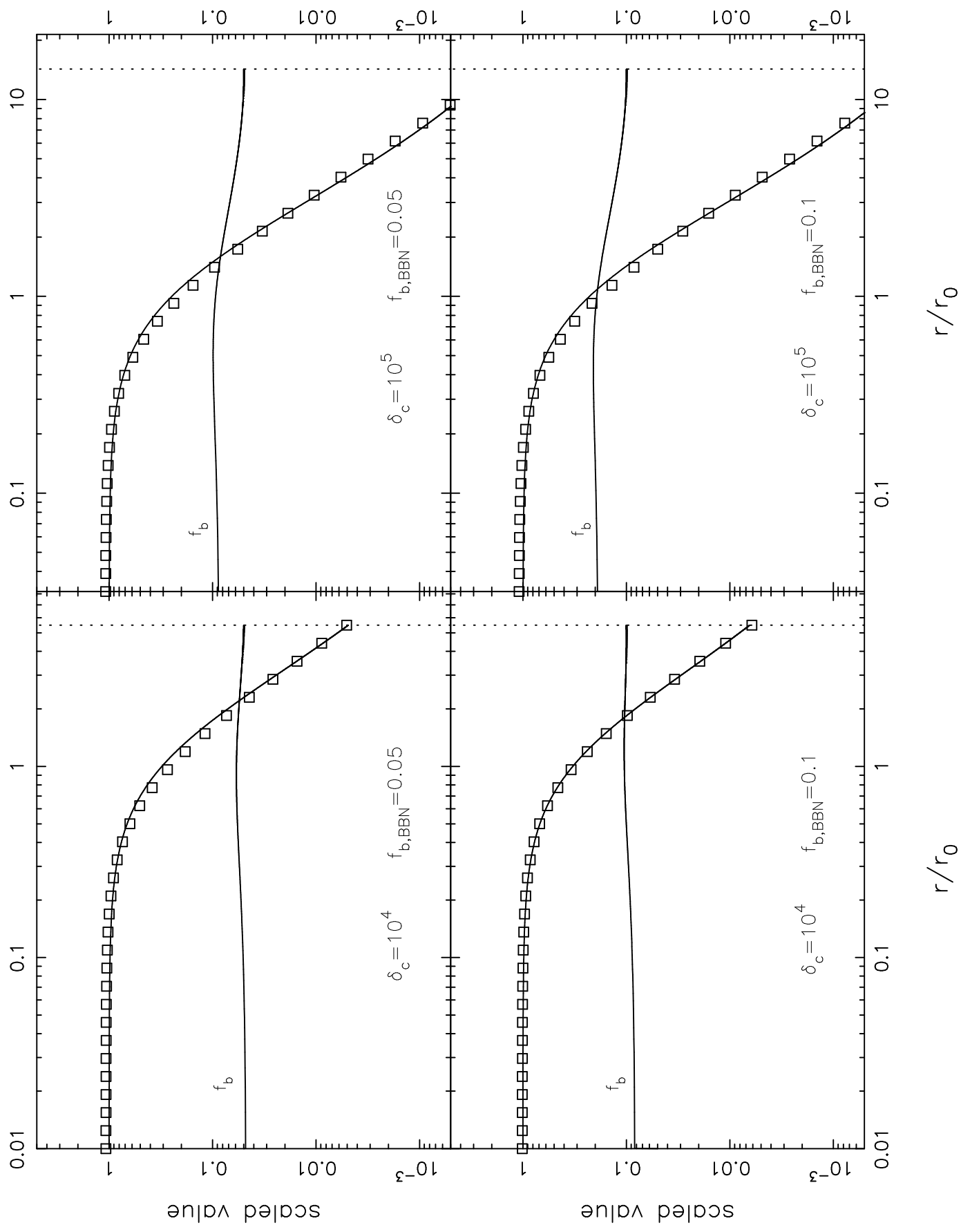


Table 2. Cluster Sample

cluster	T (keV)	r_c (Mpc)	β	α	r_s (Mpc)	ρ_s ($10^4 \rho_c$)	α_0
A85	$6.74^{+0.50}_{-0.50}$	$0.074^{+0.003}_{-0.003}$	$0.562^{+0.005}_{-0.005}$	$8.502^{+0.117}_{-0.117}$	$0.359^{+0.021}_{-0.021}$	$1.942^{+0.395}_{-0.395}$	$8.795^{+0.128}_{-0.128}$
A119	$6.05^{+0.55}_{-0.43}$	$0.514^{+0.029}_{-0.029}$	$0.714^{+0.025}_{-0.025}$	$14.977^{+1.561}_{-1.561}$	$3.238^{+0.480}_{-0.480}$	$0.038^{+0.019}_{-0.018}$	$9.056^{+0.288}_{-0.288}$
A262	$2.29^{+0.12}_{-0.09}$	$0.021^{+0.002}_{-0.002}$	$0.465^{+0.007}_{-0.007}$	$6.885^{+0.107}_{-0.107}$	$0.099^{+0.008}_{-0.008}$	$6.986^{+1.623}_{-1.532}$	$7.164^{+0.121}_{-0.121}$
A401	$10.68^{+1.11}_{-0.94}$	$0.253^{+0.007}_{-0.007}$	$0.613^{+0.005}_{-0.005}$	$8.604^{+0.100}_{-0.100}$	$0.854^{+0.030}_{-0.030}$	$0.551^{+0.102}_{-0.093}$	$8.427^{+0.064}_{-0.064}$
A426	$7.71^{+0.29}_{-0.37}$	$0.041^{+0.003}_{-0.003}$	$0.537^{+0.007}_{-0.007}$	$7.959^{+0.105}_{-0.105}$	$0.192^{+0.013}_{-0.013}$	$7.276^{+1.319}_{-1.395}$	$8.299^{+0.114}_{-0.114}$
A478	$7.42^{+0.71}_{-0.54}$	$0.111^{+0.005}_{-0.005}$	$0.663^{+0.008}_{-0.008}$	$9.529^{+0.103}_{-0.103}$	$0.406^{+0.018}_{-0.018}$	$1.874^{+0.362}_{-0.319}$	$9.909^{+0.124}_{-0.124}$
A496	$4.51^{+0.17}_{-0.15}$	$0.042^{+0.002}_{-0.002}$	$0.539^{+0.005}_{-0.005}$	$8.152^{+0.116}_{-0.116}$	$0.204^{+0.014}_{-0.014}$	$3.860^{+0.715}_{-0.698}$	$8.510^{+0.131}_{-0.131}$
A644	$7.47^{+0.32}_{-0.10}$	$0.203^{+0.011}_{-0.011}$	$0.701^{+0.015}_{-0.015}$	$10.153^{+0.311}_{-0.311}$	$0.738^{+0.055}_{-0.055}$	$0.609^{+0.136}_{-0.118}$	$9.355^{+0.070}_{-0.070}$
A754	$12.85^{+1.77}_{-1.35}$	$0.481^{+0.027}_{-0.027}$	$0.746^{+0.022}_{-0.022}$	$10.689^{+0.221}_{-0.221}$	$1.646^{+0.067}_{-0.067}$	$0.222^{+0.053}_{-0.046}$	$9.794^{+0.275}_{-0.275}$
A780	$4.49^{+0.41}_{-0.37}$	$0.072^{+0.004}_{-0.004}$	$0.636^{+0.008}_{-0.008}$	$9.203^{+0.093}_{-0.093}$	$0.270^{+0.012}_{-0.012}$	$2.475^{+0.468}_{-0.446}$	$9.640^{+0.115}_{-0.115}$
A1060	$3.27^{+0.11}_{-0.09}$	$0.089^{+0.004}_{-0.004}$	$0.608^{+0.011}_{-0.011}$	$8.970^{+0.198}_{-0.198}$	$0.337^{+0.018}_{-0.018}$	$1.127^{+0.185}_{-0.178}$	$8.263^{+0.133}_{-0.133}$
A1367	$3.99^{+0.48}_{-0.48}$	$0.449^{+0.022}_{-0.022}$	$0.717^{+0.024}_{-0.024}$	$19.753^{+2.841}_{-2.841}$	$3.969^{+0.719}_{-0.719}$	$0.022^{+0.014}_{-0.014}$	$9.104^{+0.292}_{-0.292}$
A1651	$7.15^{+0.84}_{-0.62}$	$0.160^{+0.009}_{-0.009}$	$0.637^{+0.013}_{-0.013}$	$9.055^{+0.203}_{-0.203}$	$0.556^{+0.035}_{-0.035}$	$0.914^{+0.244}_{-0.216}$	$8.643^{+0.066}_{-0.066}$
A1656	$10.03^{+0.89}_{-0.81}$	$0.361^{+0.007}_{-0.007}$	$0.665^{+0.008}_{-0.008}$	$15.386^{+1.048}_{-1.048}$	$2.569^{+0.235}_{-0.235}$	$0.102^{+0.035}_{-0.034}$	$8.304^{+0.100}_{-0.100}$
A1689	$9.48^{+1.36}_{-0.52}$	$0.187^{+0.017}_{-0.017}$	$0.752^{+0.026}_{-0.026}$	$10.929^{+0.456}_{-0.456}$	$0.680^{+0.073}_{-0.073}$	$0.979^{+0.392}_{-0.306}$	$10.099^{+0.102}_{-0.102}$
A1795	$7.26^{+0.51}_{-0.40}$	$0.112^{+0.005}_{-0.005}$	$0.687^{+0.007}_{-0.007}$	$10.140^{+0.133}_{-0.133}$	$0.470^{+0.022}_{-0.022}$	$1.458^{+0.257}_{-0.235}$	$10.401^{+0.143}_{-0.143}$
A2029	$8.22^{+0.58}_{-0.20}$	$0.101^{+0.006}_{-0.006}$	$0.633^{+0.010}_{-0.010}$	$9.124^{+0.137}_{-0.137}$	$0.379^{+0.022}_{-0.022}$	$2.288^{+0.467}_{-0.361}$	$9.438^{+0.147}_{-0.147}$
A2052	$3.30^{+0.16}_{-0.13}$	$0.052^{+0.004}_{-0.004}$	$0.588^{+0.010}_{-0.010}$	$8.463^{+0.148}_{-0.148}$	$0.195^{+0.013}_{-0.013}$	$3.204^{+0.633}_{-0.603}$	$8.624^{+0.147}_{-0.147}$
A2063	$3.90^{+0.51}_{-0.38}$	$0.097^{+0.006}_{-0.006}$	$0.572^{+0.010}_{-0.010}$	$8.073^{+0.145}_{-0.145}$	$0.337^{+0.020}_{-0.020}$	$1.208^{+0.321}_{-0.281}$	$8.061^{+0.122}_{-0.122}$
A2142	$10.96^{+2.56}_{-1.58}$	$0.192^{+0.009}_{-0.009}$	$0.643^{+0.009}_{-0.009}$	$9.200^{+0.114}_{-0.114}$	$0.699^{+0.031}_{-0.031}$	$0.901^{+0.302}_{-0.222}$	$9.264^{+0.048}_{-0.048}$
A2199	$4.70^{+0.13}_{-0.15}$	$0.067^{+0.002}_{-0.002}$	$0.600^{+0.003}_{-0.003}$	$8.979^{+0.081}_{-0.081}$	$0.307^{+0.012}_{-0.012}$	$1.954^{+0.226}_{-0.234}$	$9.353^{+0.096}_{-0.096}$
A2204	$8.18^{+1.08}_{-1.08}$	$0.060^{+0.006}_{-0.006}$	$0.587^{+0.009}_{-0.009}$	$8.525^{+0.111}_{-0.111}$	$0.226^{+0.016}_{-0.016}$	$5.985^{+1.732}_{-1.732}$	$8.962^{+0.125}_{-0.125}$
A2244	$8.47^{+0.43}_{-0.42}$	$0.111^{+0.011}_{-0.011}$	$0.587^{+0.016}_{-0.016}$	$8.119^{+0.229}_{-0.229}$	$0.354^{+0.037}_{-0.037}$	$2.398^{+0.690}_{-0.687}$	$8.299^{+0.152}_{-0.152}$
A2255	$7.76^{+1.01}_{-1.01}$	$0.603^{+0.043}_{-0.043}$	$0.817^{+0.039}_{-0.039}$	$19.756^{+4.078}_{-4.078}$	$4.571^{+1.238}_{-1.238}$	$0.032^{+0.028}_{-0.028}$	$10.280^{+0.451}_{-0.451}$
A2256	$8.69^{+1.06}_{-1.06}$	$0.446^{+0.018}_{-0.018}$	$0.779^{+0.016}_{-0.016}$	$11.941^{+0.546}_{-0.546}$	$1.768^{+0.155}_{-0.155}$	$0.145^{+0.050}_{-0.050}$	$10.047^{+0.157}_{-0.157}$

Table 2—Continued

cluster	T (keV)	r_c (Mpc)	β	α	r_s (Mpc)	ρ_s ($10^4 \rho_c$)	α_0
A2319	$13.60^{+2.22}_{-2.22}$	$0.251^{+0.014}_{-0.014}$	$0.588^{+0.012}_{-0.012}$	$8.567^{+0.221}_{-0.221}$	$0.932^{+0.063}_{-0.063}$	$0.586^{+0.190}_{-0.190}$	$7.742^{+0.085}_{-0.085}$
A2597	$3.91^{+0.27}_{-0.22}$	$0.067^{+0.004}_{-0.004}$	$0.660^{+0.011}_{-0.011}$	$9.243^{+0.164}_{-0.164}$	$0.215^{+0.017}_{-0.017}$	$3.402^{+0.822}_{-0.778}$	$9.640^{+0.159}_{-0.159}$
A3112	$4.69^{+0.27}_{-0.26}$	$0.054^{+0.004}_{-0.004}$	$0.572^{+0.007}_{-0.007}$	$8.330^{+0.081}_{-0.081}$	$0.205^{+0.010}_{-0.010}$	$4.050^{+0.680}_{-0.672}$	$8.839^{+0.100}_{-0.100}$
A3158	$8.33^{+1.43}_{-0.95}$	$0.245^{+0.017}_{-0.017}$	$0.643^{+0.019}_{-0.019}$	$9.485^{+0.521}_{-0.521}$	$0.904^{+0.108}_{-0.108}$	$0.422^{+0.197}_{-0.172}$	$8.353^{+0.133}_{-0.133}$
A3266	$9.69^{+0.97}_{-0.92}$	$0.510^{+0.024}_{-0.024}$	$0.802^{+0.021}_{-0.021}$	$12.315^{+0.328}_{-0.328}$	$2.011^{+0.096}_{-0.096}$	$0.129^{+0.029}_{-0.028}$	$10.311^{+0.234}_{-0.234}$
A3391	$6.90^{+1.47}_{-0.86}$	$0.167^{+0.015}_{-0.015}$	$0.512^{+0.016}_{-0.016}$	$7.221^{+0.308}_{-0.308}$	$0.572^{+0.066}_{-0.066}$	$0.665^{+0.323}_{-0.264}$	$6.732^{+0.145}_{-0.145}$
A3526	$4.04^{+0.11}_{-0.11}$	$0.012^{+0.001}_{-0.001}$	$0.462^{+0.005}_{-0.005}$	$6.979^{+0.081}_{-0.081}$	$0.066^{+0.004}_{-0.004}$	$28.350^{+4.967}_{-4.967}$	$7.377^{+0.102}_{-0.102}$
A3532	$4.40^{+4.70}_{-1.30}$	$0.234^{+0.020}_{-0.020}$	$0.599^{+0.024}_{-0.024}$	$9.467^{+0.742}_{-0.742}$	$0.992^{+0.148}_{-0.148}$	$0.185^{+0.267}_{-0.124}$	$7.397^{+0.158}_{-0.158}$
A3558	$6.60^{+0.50}_{-0.50}$	$0.165^{+0.007}_{-0.007}$	$0.543^{+0.007}_{-0.007}$	$7.617^{+0.098}_{-0.098}$	$0.560^{+0.023}_{-0.023}$	$0.699^{+0.121}_{-0.121}$	$7.342^{+0.054}_{-0.054}$
A3562	$6.96^{+1.77}_{-0.95}$	$0.103^{+0.006}_{-0.006}$	$0.482^{+0.006}_{-0.006}$	$6.763^{+0.090}_{-0.090}$	$0.358^{+0.020}_{-0.020}$	$1.609^{+0.614}_{-0.424}$	$6.924^{+0.062}_{-0.062}$
A3571	$8.12^{+0.42}_{-0.39}$	$0.183^{+0.009}_{-0.009}$	$0.641^{+0.011}_{-0.011}$	$9.169^{+0.189}_{-0.189}$	$0.644^{+0.037}_{-0.037}$	$0.785^{+0.148}_{-0.145}$	$8.554^{+0.051}_{-0.051}$
A3667	$8.11^{+0.82}_{-0.73}$	$0.303^{+0.017}_{-0.017}$	$0.588^{+0.012}_{-0.012}$	$8.681^{+0.269}_{-0.269}$	$1.152^{+0.088}_{-0.088}$	$0.232^{+0.066}_{-0.063}$	$7.913^{+0.147}_{-0.147}$
A4038	$3.30^{+1.60}_{-0.80}$	$0.059^{+0.004}_{-0.004}$	$0.551^{+0.010}_{-0.010}$	$7.742^{+0.134}_{-0.134}$	$0.201^{+0.013}_{-0.013}$	$2.773^{+1.747}_{-1.075}$	$7.852^{+0.115}_{-0.115}$
A4059	$4.05^{+0.23}_{-0.19}$	$0.090^{+0.005}_{-0.005}$	$0.589^{+0.011}_{-0.011}$	$8.343^{+0.156}_{-0.156}$	$0.314^{+0.019}_{-0.019}$	$1.500^{+0.296}_{-0.281}$	$8.311^{+0.135}_{-0.135}$
AWM7	$3.96^{+0.16}_{-0.14}$	$0.099^{+0.006}_{-0.006}$	$0.607^{+0.012}_{-0.012}$	$8.863^{+0.184}_{-0.184}$	$0.380^{+0.023}_{-0.023}$	$1.064^{+0.197}_{-0.191}$	$8.643^{+0.147}_{-0.147}$
Cygnus	$9.49^{+0.23}_{-0.23}$	$0.021^{+0.003}_{-0.003}$	$0.468^{+0.005}_{-0.005}$	$7.174^{+0.066}_{-0.066}$	$0.107^{+0.007}_{-0.007}$	$26.173^{+4.351}_{-4.351}$	$7.697^{+0.083}_{-0.083}$
MKW3S	$3.71^{+0.16}_{-0.19}$	$0.061^{+0.002}_{-0.002}$	$0.587^{+0.005}_{-0.005}$	$8.431^{+0.134}_{-0.134}$	$0.221^{+0.012}_{-0.012}$	$2.801^{+0.474}_{-0.496}$	$8.521^{+0.123}_{-0.123}$
OphiA	$12.74^{+0.30}_{-0.28}$	$0.175^{+0.006}_{-0.006}$	$0.644^{+0.008}_{-0.008}$	$9.201^{+0.138}_{-0.138}$	$0.614^{+0.025}_{-0.025}$	$1.359^{+0.163}_{-0.161}$	$8.539^{+0.044}_{-0.044}$
PKS0745	$8.08^{+0.54}_{-0.46}$	$0.074^{+0.004}_{-0.004}$	$0.614^{+0.007}_{-0.007}$	$8.823^{+0.094}_{-0.094}$	$0.262^{+0.013}_{-0.013}$	$4.539^{+0.814}_{-0.769}$	$9.279^{+0.108}_{-0.108}$
TriaAust	$12.48^{+3.88}_{-3.88}$	$0.285^{+0.012}_{-0.012}$	$0.640^{+0.010}_{-0.010}$	$9.436^{+0.197}_{-0.197}$	$1.069^{+0.052}_{-0.052}$	$0.451^{+0.193}_{-0.193}$	$8.408^{+0.087}_{-0.087}$
Average	$7.08^{+2.91}_{-2.91}$	$0.179^{+0.152}_{-0.152}$	$0.619^{+0.084}_{-0.084}$	$9.620^{+2.820}_{-2.820}$	$0.827^{+0.999}_{-0.999}$	$2.896^{+5.610}_{-5.610}$	$8.677^{+0.932}_{-0.932}$

